A NEURAL NETWORK APPROACH FOR REGIONAL VERTICAL TOTAL ELECTRON CONTENT MODELLING

R.F. LEANDRO AND M.C. SANTOS

Department of Geodesy and Geomatics Engineering, University of New Brunswick, P.O. Box 4400, Fredericton, N.B., E3B 5A3, Canada (r.leandro@unb.ca, msantos@unb.ca)

Received: November 8, 2005; Revised: May 14, 2006; Accepted: October 20, 2006

ABSTRACT

A Neural Network model has been developed for estimating the total electron content (TEC) of the ionosphere. TEC is proportional to the delay suffered by electromagnetic signals crossing the ionosphere and is among the errors that impact GNSS (Global Navigation Satellite Systems) observations. Ionospheric delay is particularly a problem for single frequency receivers, which cannot eliminate the (first-order) ionospheric delay by combining observations at two frequencies. Single frequency users rely on applying corrections based on prediction models or on regional models formed based on actual data collected by a network of receivers. A regional model based on a neural network has been designed and tested using data sets collected by the Brazilian GPS Network (RMBC) covering periods of low and high solar activity. Analysis of the results indicates that the model is capable of recovering, on average, 85% of TEC values.

Key words: total electron content, ionosphere, regional ionospheric model, neural network

1. INTRODUCTION

Ionospheric refraction is one of the most harmful effects on GPS signals. It is proportional to the total electron content (*TEC*), which corresponds to the number of free electrons contained in the ionospheric layer (*Hofmann-Wellenhof, 2001*). *TEC* is defined as the number of free electrons contained within a one meter squared column, along the path of the signal through the ionosphere. It is a number associated with a slant trajectory with respect to the local zenith, as a function of the elevation angle of the satellite. In addition to that, the signal goes through the ionosphere at coordinates different from those of the station, at the ionospheric piercing point.

It is possible to determine the delay caused by the ionospheric refraction on a GPS signal once *TEC* is known. The refraction is a function of the frequency because of the dispersive character of the ionosphere. The delay can be determined from dual-frequency observations for the site where the receiver is located.

For single frequency receiver users, one alternative is using a regional model of *TEC*, generated by realizing measurements of a dual frequency receiver network. In general,

© 2007 StudiaGeo s.r.o., Prague

from a network of spatially distributed receivers a grid of *TEC* values can be generated. From this grid *TEC* can be inferred to any position inside or near the region covered by the tracking network, making it possible to correct the single-frequency receiver observations.

In this paper we explore a new approach to regional *TEC* modeling, using a Neural Network model.

2. COMPUTING VERTICAL *TEC* FROM DUAL-FREQUENCY RECEIVERS

The computation of Vertical *TEC* (*VTEC*), using dual frequency observations, results in the determination of *VTEC* values for each station. We are using a simple model for *VTEC* computation since our final goal is to estimate *VTEC* for void areas, i.e., for areas where there is not an observing receiver. Similar values can be computed using different techniques, probably providing better quality input data to the regional model.

The receivers located at the study area did not acquire pseudoranges at both frequencies. Only carrier phases were observed at the two GPS frequency bands. To overcome this limitation, we implemented a *TEC* computation model totally based on carrier phase observations. In this section we show the *TEC* computation model developed as part of this research, which formed the basis for the estimation using artificial neural networks.

We start by modelling the carrier-phase measurements on two frequencies (L_1 and L_2) as:

$$\lambda_1 \varphi_{r1}^s(t) = \rho_r^s(t) - I_{r1}^s(t) + T_{r1}^s(t) + \delta_{r1}^s(t)c + \lambda_1 N_{r1}^s, \tag{1}$$

$$\lambda_2 \varphi_{r2}^s(t) = \rho_r^s(t) - I_{r2}^s(t) + T_{r2}^s(t) + \delta_{r2}^s(t)c + \lambda_2 N_{r2}^s, \tag{2}$$

where λ_1 and λ_2 are the carrier phase wavelengths, in meters, $\varphi_{r1}^s(t)$ and $\varphi_{r2}^s(t)$ are carrier-phase measurements for a receiver *r* and a satellite *s*, in cycles, $\rho_r^s(t)$ is the geometric distance between receiver and satellite antennas, in meters, $I_{r1}^s(t)$ and $I_{r2}^s(t)$ represent ionospheric refraction, in meters, $T_{r1}^s(t)$ and $T_{r2}^s(t)$ represent tropospheric refraction, in meters, $\delta_{r1}^s(t)$ and $\delta_{r2}^s(t)$ are the combinations of the satellite and receiver clock errors, in seconds, *c* is the speed of light, in meters per second, and N_{r1}^s and N_{r2}^s are the carrier phase ambiguities, in cycles. The time argument is represented by *t*.

Subtracting Eq.(2) from Eq.(1) gives:

$$\lambda_2 \varphi_{r2}^s(t) - \lambda_1 \varphi_{r1}^s(t) = I_{r1}^S(t) - I_{r2}^s(t) + \lambda_2 N_{r2}^s - \lambda_1 N_{r1}^s. \tag{3}$$

The terms due to geometric distance, tropospheric delay and clock errors are cancelled out since they are the same for both frequencies. In the absence of a cycle slip the ambiguity terms are constant. The ambiguity terms on both frequencies are combined into a constant term C_r^s:

$$C_r^s = \lambda_2 N_{r2}^s - \lambda_1 N_{r1}^s . \tag{4}$$

Substituting Eq.(4) into Eq.(3) we get:

$$\lambda_2 \varphi_{r2}^s(t) - \lambda_1 \varphi_{r1}^s(t) = I_{r1}^s(t) - I_{r2}^s(t) + C_r^s . \tag{5}$$

The influence of ionosphere on GPS signals (I_{r1}^s and I_{r2}^s) can be computed by (*Hoffmann-Wellenhof, 2001*; *Leick, 2004*):

$$I_{r1}^s = \frac{40.3\,TEC}{(f_1)^2} , \tag{6}$$

and

$$I_{r2}^s = \frac{40.3\,TEC}{(f_2)^2} , \tag{7}$$

where f_1 and f_2 are the frequencies of the L_1 and L_2 carrier signals, in Hz, and *TEC* is the total electron content in electrons $\times 10^{16}$ m^{-2}. Substituting Eqs.(6) and (7) into Eq.(5), the following expression is obtained:

$$\lambda_2 \varphi_{r2}^s(t) - \lambda_1 \varphi_{r1}^s(t) = TEC\left(\frac{40.3}{(f_1)^2} - \frac{40.3}{(f_2)^2}\right) + C_r^s . \tag{8}$$

Eq.(8) can be evaluated, after elementary operations, as:

$$TEC + 9.52 C_r^s = 9.52\left(\lambda_2 \varphi_{r2}^s(t) - \lambda_1 \varphi_{r1}^s(t)\right) . \tag{9}$$

A mapping function must be used to account for the inclination and the position of the piercing point, allowing the computation of *VTEC* directly:

$$TEC = \frac{1}{\sin\nu} VTEC , \tag{10}$$

where $1/\sin\nu$ is the mapping function term that accounts for path inclination, defined as a function of the elevation angle ν of the satellite as perceived from the observing station. The function to model the latitude and longitude dependence is a bilinear model (*Komjathy and Langley, 1996*):

$$TEC = \frac{1}{\sin\nu}\left(a_0 + a_1 \Delta\phi + a_2 \Delta\lambda\right) , \tag{11}$$

where $\Delta\phi$ and $\Delta\lambda$ are differences in latitude and in longitude between the observation point and the ionospheric piercing point, respectively, and a_0, a_1 and a_2 are unknown coefficients of the bilinear model. Substituting Eq.(11) into Eq.(9) we get the final expression used in this work:

$$\frac{1}{\sin\nu}\left(a_0 + a_1 \Delta\phi + a_2 \Delta\lambda\right) + 9.52 C_r^s = 9.52\left(\lambda_2 \varphi_{r2}^s(t) - \lambda_1 \varphi_{r1}^s(t)\right) . \tag{12}$$

This expression allows computation of the coefficients a_0, a_1 and a_2, and a consequent determination of *VTEC* for the tracking stations using measurements collected for all visible satellites during a certain period of time.

The 3 coefficients as well as the term C_r^s, one for each satellite, are estimated in a least squares parametric adjustment. If a cycle slip occurs it is necessary to add another term to determine the combined ambiguities and the adjustment looses one degree of freedom. In the case of many cycle slips it may be better to ignore the satellite altogether, avoiding an excessive increase in the number of ambiguity parameters.

There will be a total of $3 + s$ unknowns, s being the number of satellites. The total number of observations is equal to the summation of all observations collected for every satellite.

For simplification we assume *TEC* is a constant value during a one-hour period. This period provides a large enough number of degrees of freedom in the adjustment to attempt to successfully estimate the parameters containing phase ambiguities. The operational restriction we faced (the receivers did not acquire pseudorange on L_2) forced us to rely solely on carrier phase measurements, causing our approach to suffer under a situation of high variation of the ionospheric activity.

At the outset there will be a *VTEC* value associated with each station of the network, valid for the one hour period used in the computation described above. The computed value of *VTEC* represents the average ionospheric activity over the one hour used in the *TEC* computation, for each of the stations. These values are the input of the Neural Network Model, which will predict *VTEC* values for any point in the region covered by the network, for the same time period (1 hour).

3. NEURAL NETWORK MODEL

A Neural Network is an information processing system formed by simple processing elements, called artificial neurons, or simply neurons. Fig. 1 shows an artificial neuron model. The input signal of the neuron is manipulated by means of synaptic weights. Synaptic weights are parameters which are adjusted during an iterative adjustment process known as training process. After the training process an activation function is applied to all neuron processes to generate the output signal. The neural network also includes a term that is applied externally, called bias, and represented in Fig. 1 by b_k. The bias has the function of increasing or decreasing the neuron input. In the case of a linear activation function, the neuron plays the role of a regression linear model. The processing of a neuron k can be represented by:

$$y_k = \Psi\left(\sum_{i=1}^{m}\left(x_i w_{ki}\right) + b_k\right), \tag{13}$$

where y is the neuron output, Ψ is the activation function, m is the number of input parameters, x is the input parameter, w is the synaptic weight and b is the bias.

The range of the normalized amplitude of a neuron process varies within the range [0,1] or [−1,1]. This range depends on the type of activation function used.

Additional layers of neurons, called hidden layers, can be introduced into the neural network. The input signal of the first hidden layer comes from the input layer. The output signal of the last hidden layer is used to generate the input signal to the output layer. A neural network model may have more than one hidden layer. The model resulting from adding hidden layers between the input and output layers is called Multilayer Perceptron (MLP). The MLP is not the only type of neural network model, but is one of the most popular ones. In this work we have used an MLP.

Once a neural network model is defined, it is necessary to train it with data. The data is composed of a set of known input and output parameters. The training process corresponds to an adjustment of the synaptic weights to the data set. This adjustment attempts to decrease the residuals (difference between the computed output and the known output) of the output of the network, by means of an update of the synaptic weights. Due to the complexity of neural networks the adjustment cannot be done on a single step. An iterative adjustment of the synaptic weights is performed, called training algorithm. One of these algorithms is the Back-Propagation Training Algorithm, which is composed of two steps. Details about neural network training process can be found in *Haykin (1999)*. A comprehensive introduction to neural network applications in geodesy and space research can be found in *Leandro and Santos (2004)* and *Tulunay et al. (2004a)*. Other types of neural network applications for ionosphere modeling are also explored in *McKinnell (2002)* and *Tulunay et al. (2004b)*.

A neural network model was designed to estimate the *VTEC* for a given position. The input parameters are latitude and longitude, while the output parameter is *VTEC*. The training parameters are the known coordinates and *VTEC* values of each station of the GPS network at a given time. Once the model is trained we can estimate a *VTEC* to any position inside or near the region covered by the GPS network to the given time. Input parameters related to time variability of ionospheric activity, such as parameters representing geomagnetic and solar activities were not used because, in this case, the neural network *VTEC* estimations are supposed to be made only for the same period in which *TEC* values were computed from the GPS receivers network. Therefore, the neural network models the regional behaviour of the ionosphere for a specific time period, in our case, of one hour.

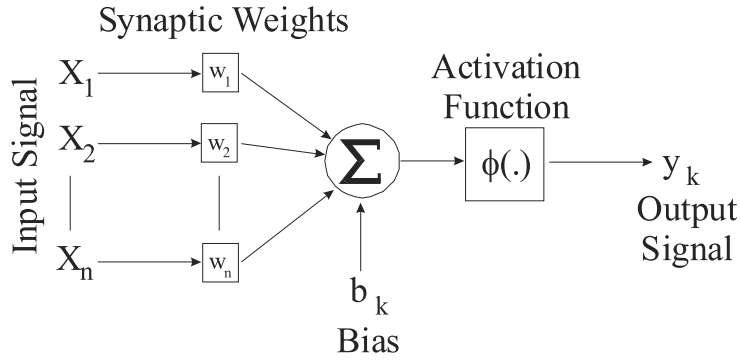

Fig. 1. Nonlinear artificial neuron model (adapted from *Haykin, 1999*).

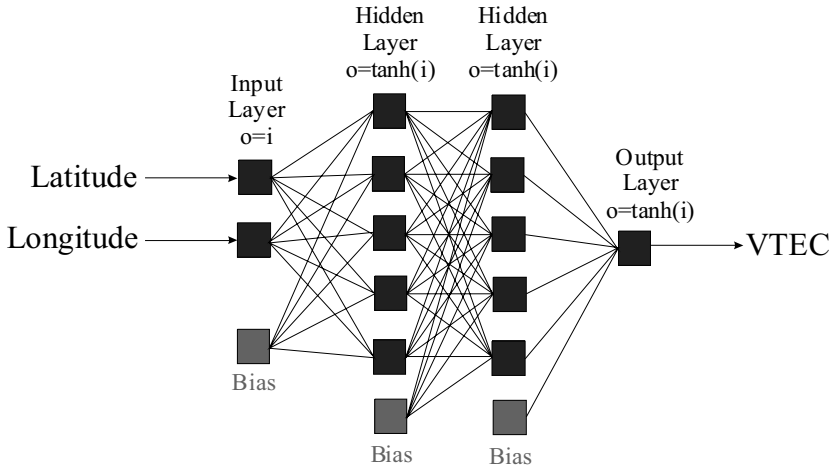

Fig. 2. The Neural Network Model.

Fig. 2 shows the scheme of the neural network model used in this investigation. Two hidden layers were used, each one with five neurons. The activation function of all layers (except the input one) is the hyperbolic tangent sigmoid function, represented by:

$$\varphi(x) = \frac{2}{1+\mathrm{e}^{-2x}} - 1, \tag{14}$$

where x is the input signal of the neuron.

The Levenberg-Marquardt back-propagation algorithm was used to train the neural model. The neural network processing was carried out in MatLab.

4. ANALYSIS STRATEGY

Data from a subset of the Brazilian active control network (RBMC) were used in this investigation. Fig. 3 shows the locations of the stations used.

The continental coverage of the network can be considered one additional challenge for testing the capability of the model to estimate *TEC* over large areas.

Fig. 4 shows a flowchart of the data processing for each given time. For each determination of *VTEC*, one of the network stations was not used during the neural network training process. This particular station became a test station. After the training process the model was used to estimate the *VTEC* value for the test station without any further modification. This estimate value is then compared with the GPS derived *VTEC* value (Eqs.(1)–(12)). The difference is the estimation error of the Neural Network Model. This procedure was repeated for each one of the 11 stations allowing us to assess the performance of the model everywhere in the study area.

The training and testing procedure was performed for each isolated station using two different periods of five days each. The first was a period of low solar activity (from February 1st to February 5th 2004) and the other was a period of high solar activity (from

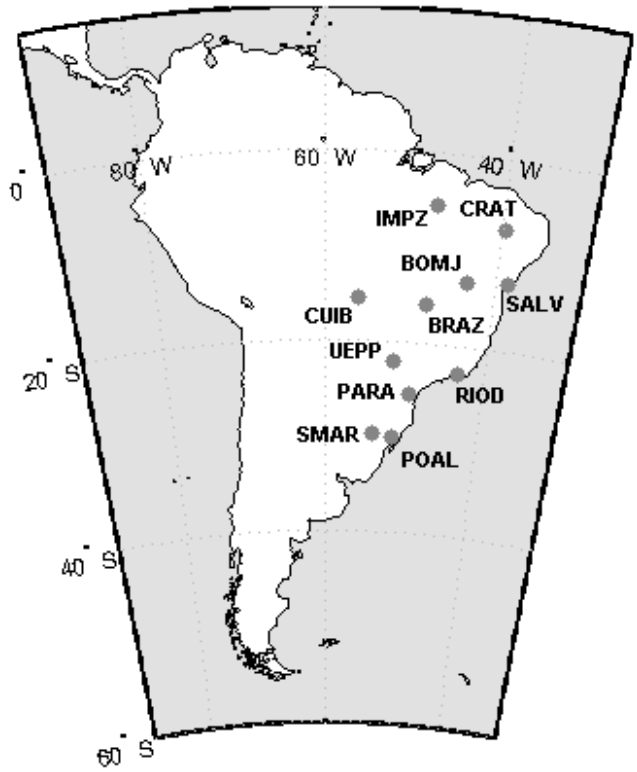

Fig. 3. Stations of the RBMC.

October 26th to October 30th 2003). Fig. 5 shows the solar radio flux for years of 2003 and 2004. The days used as low solar activity period are shown as circles and the ones used for high solar activity are shown as triangles.

For each day *VTEC* values were computed at 12:00 LT, 14:00 LT and 16:00 LT (where LT stands for local time), corresponding to three training and testing procedures per day per station. These times of the day were chosen in order to test the model near the time of the day with higher ionospheric activities, around 12:00 LT according to *Klobuchar (1987)*. According to this procedure the total number of estimations would be 330 for the 11 stations, however, due to the absence of data of some stations for some of the days used, 318 estimations were performed in total. As mentioned before, the period used for *TEC* computation was 1 hour.

Due to the small number of receivers and the procedure adopted for *TEC* computation, the number of patterns available to be used in the neural process was small. A total of 10 patterns were used for training the model, each one related to one of the receivers of the network. Because of this limitation the use of a test set (set of patterns used prior to the estimations to verify the generalization capability of the model) was not possible. However the results show that the generalization capability of the model is good, even with stations poorly distributed across the region.

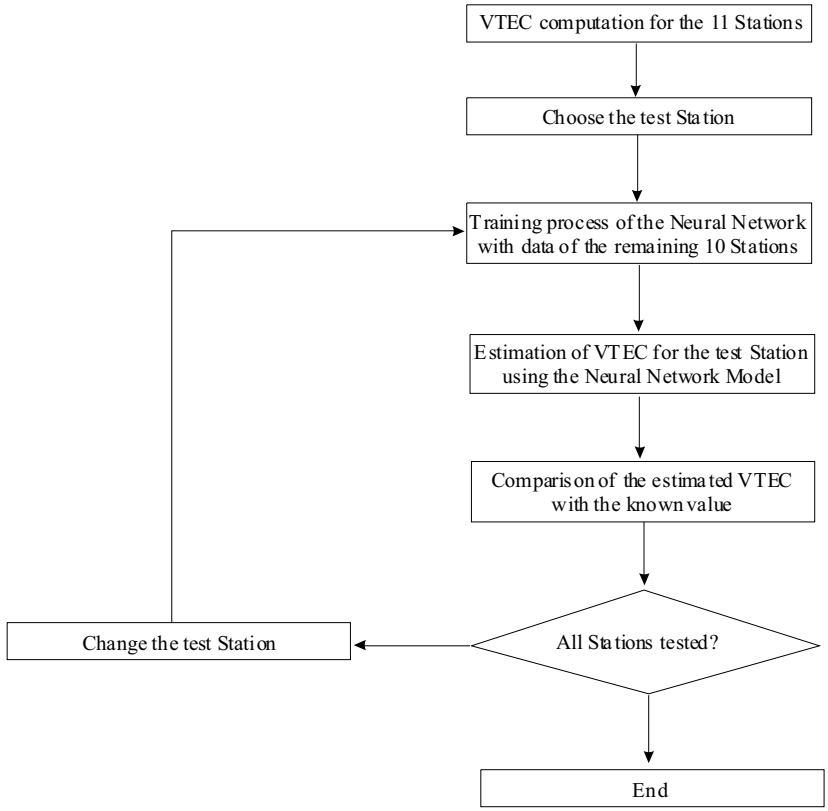

Fig. 4. Flowchart of the data processing.

5. ASSESSMENT OF RESULTS

In our analysis we assessed both absolute and relative errors. The absolute error $|\alpha|$ can be computed according to:

$$|\alpha| = |VTEC_e - VTEC|, \tag{15}$$

where α represents the error in the estimation of $VTEC_e$. VTEC represents the value computed from GPS observations using the dual-frequency algorithm described in Section 2, and $VTEC_e$ is the predicted value of *VTEC* as computed using the Neural Network model presented in Section 3. Both quantities are expressed in units of *TEC* (TECU). The relative error ε can be computed according to:

$$\varepsilon = \frac{|\alpha|}{VTEC} \times 100 . \tag{16}$$

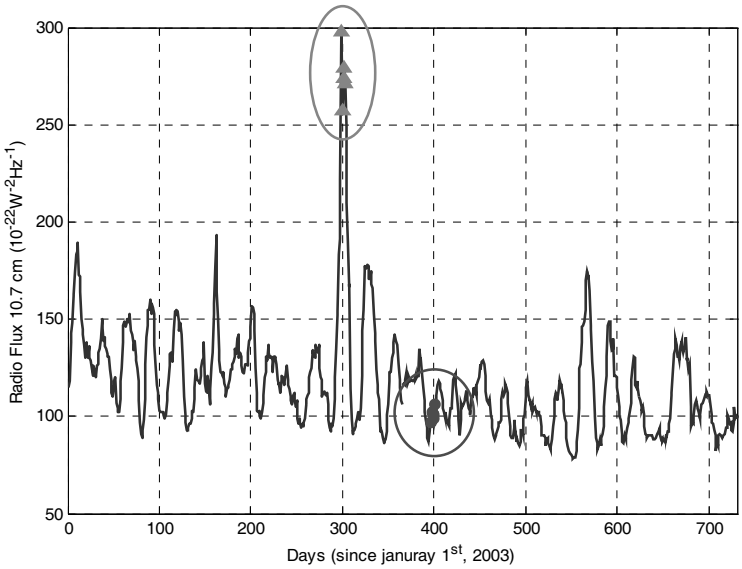

Fig. 5. Solar activity for years of 2003 and 2004 (*Space Environment Center, 2004*).

The less the absolute and relative errors are, the closer $VTEC_e$ and *VTEC* are. Ionospheric delay can be corrected with an accuracy similar to the estimation of *TEC* due to the direct relationship between *TEC* and ionospheric delay. Therefore, accuracy of *VTEC* estimation can be considered the same as the accuracy of correcting ionospheric delay to single frequency receivers.

In this investigation a total of 318 estimations were made with the neural network model, involving different station configurations, days and times of day. Half of those estimations were made for a period with low solar activity whereas the other half were performed when the sun was very active. The results are grouped in order to compare the GPS-derived values of *VTEC* with the ones originating from the Neural Network solution VTECe. This comparison is provided in terms of the mean error α and the mean absolute error $|\alpha|$, as given by Eq.(15), the relative error ε, as given by Eq.(16), and the relative correction (100% – ε). For the sake of this comparison, the GPS-derived values of *VTEC* are considered as a bench mark. The differences found indicate the error in the values of $VTEC_e$. The mean error (α) shows the mean bias of the estimations with respect to the known values of *VTEC*. The mean absolute error $|\alpha|$ gives a quantity for the average estimation error as well as for its standard deviation. Standard deviation and RMS are given in 1-sigma values.

Table 1 summarizes the results obtained for the low solar activity period. The difference between mean *VTEC* and mean $VTEC_e$, i.e., the mean error α equals 0.4 TECU, which corresponds to approximately 7 cm of delay at the L_1 frequency. Since α (which could be considered as a bias) is very small, the spread of the difference as given by both the *RMS* and the standard deviation is almost the same. The minimum and maximum

Table 1. Statistics of the solutions obtained during the low solar activity period.

	VTEC [TECU]	$VTEC_e$ [TECU]	α [TECU]	$\lvert\alpha\rvert$ [TECU]	ε [%]	$100-\varepsilon$ [%]
Mean	18.7	19.1	0.4	3.0	16.7	83.3
Std. Dev.	4.7	4.4	3.7	2.0	11.4	11.4
RMS	-	-	3.6		20.1	-
Minimum	12.4	12.6	–5.9	0.2	1.4	62.2
Maximum	32.2	29.0	5.7	5.9	37.8	98.6

values (–5.9 and 5.7) indicate a possible symmetry in the differences between mean *VTEC* and mean $VTEC_e$. The mean absolute error $\lvert\alpha\rvert$ of the estimation is 3 TECU with standard deviation of 2 TECU. In terms of relative error ε it was found an average value of 16.7%. Alternatively, indicating an agreement in 83.3% of the cases.

Table 2 summarizes the results obtained for the high solar activity period. The difference of mean *VTEC* and mean $VTEC_e$, i.e., the mean error α equals to –1.1 TECU, which corresponds to approximately 18 cm of delay at the L_1 frequency. This values is more than twice the one for the low solar activity period. The spread of the difference as given by both the *RMS* and the standard deviation is still almost the same because α is still a small value. The minimum and maximum values (–9.1 and 8.4) again seem to suggest a possible symmetry in the differences between mean values of *VTEC* and $VTEC_e$. The module of the mean absolute error $\lvert\alpha\rvert$ of the estimation is 4.3 TECU with standard deviation of 3.1 TECU. The maximum error of all estimations is 9.1 TECU. In terms of relative error ε it was found that the estimations had error of 13.2% in average. Alternatively, this indicates an agreement in 86.1% of the cases. Although the absolute errors are greater for higher solar activity period, the relative errors are less than that for the period of low solar activity. This is an artifact due to the higher values of *TEC* as an outcome of the high activity itself.

Table 3 summarizes the overall results achieved in this investigation, involving all results both for low and high solar activity. The average absolute error of all estimations is

Table 2. Statistics of the solutions obtained during the high solar activity period.

	VTEC [TECU]	$VTEC_e$ [TECU]	α [TECU]	$\lvert\alpha\rvert$ [TECU]	ε [%]	$100-\varepsilon$ [%]
Mean	35.4	34.3	–1.1	4.3	13.2	86.8
Std. Dev.	9.7	9.1	5.3	3.1	10.3	10.3
RMS	-	-	5.3	-	16.6	-
Minimum	20.6	20.9	–9.1	0.1	0.3	68.1
Maximum	60.0	59.7	8.4	9.1	31.9	99.7

Table 3. Synopsis of the results.

	VTEC [TECU]	$VTEC_e$ [TECU]	α [TECU]	$\lvert\alpha\rvert$ [TECU]	ε [%]	$100 - \varepsilon$ [%]
Mean	27.4	27.1	-0.4	3.7	14.9	85.1
Std. Dev.	11.4	10.5	4.56	2.7	10.9	10.9
RMS	-	-	4.6	-	18.7	-

equal to 3.7 TECU with standard deviation of 2.7 TECU. The average relative error was 14.9%, with standard deviation of 10.9%. This indicates that the average relative correction of ionospheric delays that would be made possible by using our technique would be at least around 85%.

Looking at the results in terms of geographical location it can be seen that there are a few differences for each station individually. Figs. 6 and 7 show the mean absolute errors obtained for each station used during the low and the high solar activity periods, respectively. The errors obtained for the period of higher solar activities are obviously greater than those for the lower solar activities, with maximum values around double the value from the latter. In both situations, smaller errors were found for stations situated around the 15° latitude South, exactly those not affected by the equatorial electrojet and by the South Atlantic Anomaly. These stations are also located near the center of the region, where better estimation performances are expected. The largest errors are more readily noticed for the stations on the equatorial electrojet path (CRAT and IMPZ) followed by those under the influence of the South Atlantic Anomaly (especially PARA). The lowest errors were found for stations CUIB and BRAZ, during both low and high solar activities, respectively.

The case of station IMPZ requires further explanation. Since we tested the performance of the model by data deprivation, whenever we removed a station located at the border of the region, the situation became a case of extrapolation. Station IMPZ is the farthest station from the rest of the stations of the network. Also, it is located along the path of the equatorial electrojet. We believe that this combination of extrapolation error plus the effect of the equatorial electrojet explains very well the large absolute error value it shows. A similar effect impacted station CRAT. Looking a little into the South, an analogous reasoning can be used for station PARA. The neighboring stations at the border of the region show an absolute error smaller than station PARA, but station PARA is under the direct influence of the South Atlantic Anomaly.

An expected feature that we can observe from Figs. 6 and 7 is that stations within the network have the lowest absolute error values. This is particularly noticeable for station BRAZ, which has an absolute error value of around 1 TECU even during high solar activity.

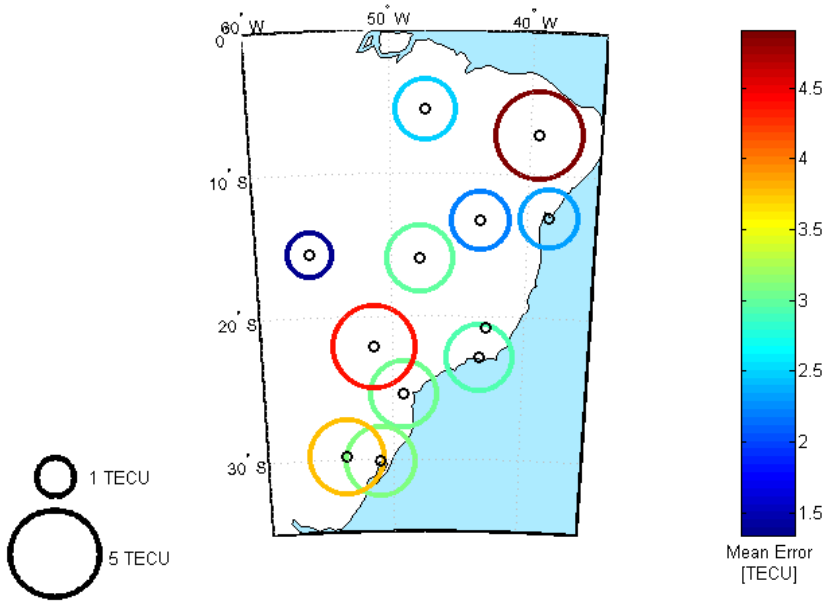

Fig. 6. Mean absolute errors by location for a low solar activity period.

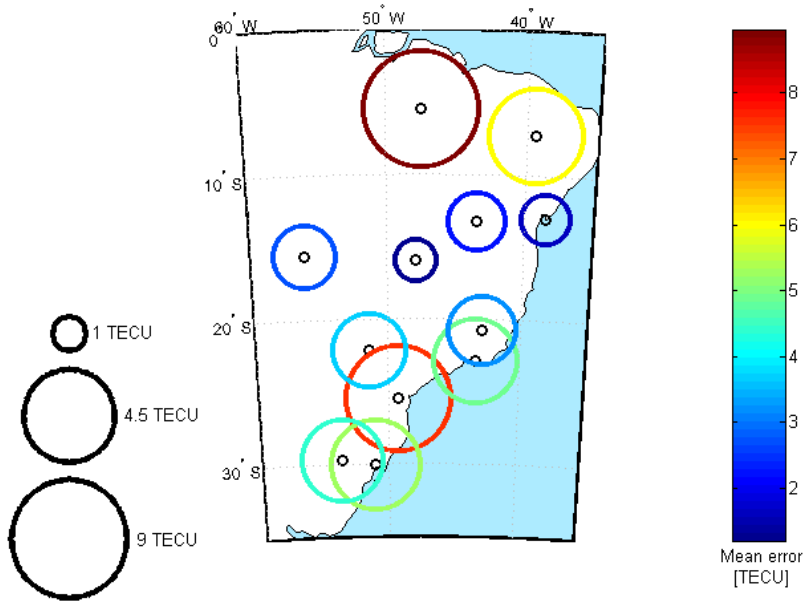

Fig. 7. Mean absolute errors by location for a high solar activity period.

6. CONCLUSIONS AND FUTURE RESEARCH

The Neural Network model provided estimates of *VTEC* values with an average absolute error of 3.7 TECU with standard deviation of 2.7 TECU (1 sigma). The average relative error was 14.9%, with standard deviation of 10.9% (1 sigma).

The worst absolute error results were obtained in periods of high solar activity. The worst relative error results were obtained in periods of low solar activity, due to a lower absolute *TEC* value during low solar activity periods. In absolute terms the performance of the Neural Network model was better during low solar activity periods (3.1 TECU and 4.3 TECU, respectively).

The worst average error results were obtained for station IMPZ for two reasons. It lies under the equatorial electrojet and, being the farthest from the others, when used as test station it was located outside the region formed by the stations used in the training process.

According to these preliminary results the Neural Network model can correct approximately 85% of the ionospheric refraction, providing values which can be used by single frequency receivers located inside or near the borders of the network region. We believe that these results can be improved if a more comprehensive manipulation of the input data set is carried out. This would bring improvements to the estimations. In this paper, the technique used to compute *TEC* values for each station is not an optimal approach, because it depends on an ambiguity term that is not fixed. Data from other regions can also show different performances when using this technique.

Even though the distribution of tracking stations in the network used in this research is sparse, the model produced good estimations. With a larger number of stations we expect an improved stability and reliability of the model estimations. further research is underway using data sets generated with more dense GPS networks and with larger geographical coverage. Our further research also involves the estimation of *VTEC* values for real time scenarios.

We used five days periods of high and low solar activity which were only about six months apart from each other. For future research it would also be interesting to compare measured and predicted *TEC* values over a larger time periods.

Aknowledgements: Funding for this work was partially provided by the National Science and Engineering Research Council of Canada. We acknowledge also the anonymous reviewers for their useful comments.

References

Haykin S., 1999. *Neural Networks - A Comprehensive Foundation*. Prentice Hall, Upper Saddle River, New Jersey, USA.

Hoffmann-Wellenhof B., Lichteneeger H. and Collins J., 2001. *Global Positioning System: Theory and Practice*. Springer-Verlag, Wien, New York.

Klobuchar J.A., 1987. Ionospheric time-delay algorithm for single-frequency GPS users. *IEEE Trans. Aerosp. Electron. Syst.*, **23**, 325–331.

Komjathy A., 1997. *Global Ionospheric Total Electron Content Mapping Using the Global Positioning System*. Ph.D. Thesis, Department of Geodesy and Geomatics Engineering Technical Report No. 188, University of New Brunswick, Fredericton, New Brunswick, Canada.

Leandro R.F. and Santos M.C., 2004. Comparison between autoregressive model and neural network for forecasting space environment parameters. *Bollettino di Geodesia e Scienze Affini*, **LXII**, N.3, 197–212.

Leick A., 2004. *GPS Satellite Surveying*. John Wiley and Sons, Hoboken, New Jersey, USA.

McKinnell L., 2002. *A Neural Network Based Ionospheric Model for the Bottomside Electron Density Profile over Grahamstown, South Africa*. Ph.D. Thesis, Rhodes University, Grahamstown, South Africa.

Space Environment Center, 2004. http://www.sec.noaa.gov/ftpmenu/indices/old_indices.html, accessed March 1st.

Tulunay Y., Tulunay E. and Senalp E.T., 2004a. The neural network technique-1: a general exposition. *Adv. Space Res.*, **33**, 983–987.

Tulunay Y., Tulunay E. and Senalp E.T., 2004b. The neural network technique-2: an ionospheric example illustrating its application. *Adv. Space Res.*, **33**, 988–992.